

Mechanisms for Laser Control of Chemical Reactions

Ben R. Torralva and Roland E. Allen

*Department of Physics, Texas A&M University,
College Station, Texas 77843, USA*

Abstract

During the past several years our group has developed and employed a new technique for realistic simulations of the interaction of light with matter. Recent simulations of laser pulses interacting with molecules clearly demonstrate the potential for control of chemical reactions, through various mechanisms which include the following: (i) excitation of electrons to states which have different bonding properties; (ii) control of electron populations through a coherent pump-pulse, control-pulse sequence; and (iii) control of molecular vibrations through a pump-control sequence. Significant chemical insights are gained when one can watch a realistic animation of species interacting and reacting. One can monitor the time evolution of electronic states and their occupancy, as well as the motion of the atoms. One can also observe the evolution from reactants to products through transition states. Finally, one can determine how this evolution is affected by the various properties of the laser pulses, including intensity, duration, phase, and the interval between pulses.

1 Introduction

For decades, chemists have dreamed of using lasers to selectively control chemical reactions. It was initially believed that by properly tuning the laser to the local mode frequency corresponding to a specific chemical bond, enough energy could be deposited to break the bonds selectively, and consequently drive a chemical reaction which would not normally occur or which only occurs inefficiently. In practice, however, it became clear that, except for the smallest molecules, the energy deposited rapidly redistributes throughout the molecule, destroying the selectivity [1]. On the other hand, developments in laser technology, together with an understanding that the explicit quantum nature of the system must be recognized and exploited (through, e.g., constructive and destructive interference), have permitted recent progress in manipulating larger systems on an atomic scale.

The improvements in laser technology that have led to a rapid increase in activity in this area of chemistry are the following: (i) the development of laser systems capable of producing ultrashort pulses, allowing the energy of the electromagnetic field to be delivered in as little as 4.5 fs; (ii) the ability to tailor the frequency, envelope, and phase of pulses, so that they can be designed to bring about some specific change in the molecular system; and (iii) the ability to produce phase-locked pulse trains, with multiple pulses time-delayed,

so that one pulse will either constructively or destructively interfere with the state set in motion by a preceding pulse.

We will address two of the three major types of experiments in what has become known as the field of femtochemistry. First, we will present simulations in which a single pulse is used to bring about a specific change in an organic system. In practice, these are carried out as pump-probe experiments, where the pump pulse is used to facilitate a chemical reaction and a probe pulse is used to monitor the subsequent real-time quantum dynamics. In our simulations we can monitor the system directly, and we will report on the dynamics of the system, as well as the occupancy of the excited states and the kinetic energy. The second type of simulation that we present in this paper is one in which a phase-locked pump-pulse, control-pulse pair is separated by a variable time delay, whose value is tuned to achieve either constructive or destructive interference in the quantum dynamics of the electrons, or in the vibrational motion of the atoms.

The technique used for our simulations is density-functional-based tight-binding electron dynamics (DFTED) [2-8]. We have provided a complete description of this technique elsewhere [5, 6]. Here we mention only the following features: (a) The vector potential $\mathbf{A}(\mathbf{x}, t)$ for the radiation field is included in the electronic Hamiltonian \mathbf{H} through a time-dependent Peierls substitution. (b) The time-dependent Schrödinger equation is solved with an algorithm that conserves probability and satisfies the Pauli exclusion principle. (c) The atomic forces are obtained from a generalized Hellmann-Feynman theorem, which may also be interpreted as a generalized Ehrenfest theorem. (d) The method is accurate and computationally efficient because it is based on a simplified form of density functional theory [9-12].

With the present approach, one can investigate potential mechanisms for laser control of chemical reactions, through realistic simulations which reveal in microscopic detail how the reacting molecules are affected by changes in the laser-pulse parameters: for example, the intensity and duration of each pulse, and the time interval between pump and control pulses.

In these initial studies, we examine four mechanisms:

- Promotion of electrons to excited states with different bonding properties – so that, e.g., a symmetry-forbidden reaction becomes symmetry-allowed. In this paper we specifically consider photoinduced cycloaddition of ethylene molecules and selective photodissociation of cyclobutane.

- Photoisomerization of a molecule – a change of molecular structure resulting from the absorption of radiation. Here we specifically consider photoisomerization of butadiene.

- Control of electron populations through a pump-pulse, control-pulse sequence. The specific molecule treated here is benzene.

- Control of molecular vibrations through a pump-control sequence. Again, the present simulations are specifically for benzene.

Let us now turn to a detailed discussion of our results for each of the above processes.

2 Photoinduced 2+2 Cycloaddition

The idea of conservation of orbital symmetry, introduced by Woodward and Hoffmann [13], has been shown to be a powerful tool in understanding whether a given reaction will proceed

according to lowest-order symmetry considerations. The main idea is that reactions proceed readily if there is congruence between orbital symmetry characteristics of reactants and products.

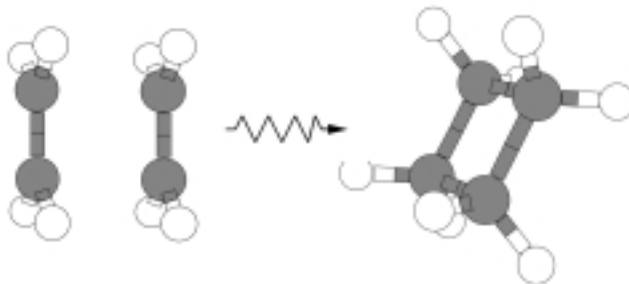


Figure 1: The formation of cyclobutane from two molecules of ethylene is a symmetry-forbidden reaction. However, through the photoexcitation of electrons to antibonding orbitals, the reaction can be made symmetry-allowed. The above is a schematic drawing, and results from a realistic computer simulation are shown in Fig. 9.

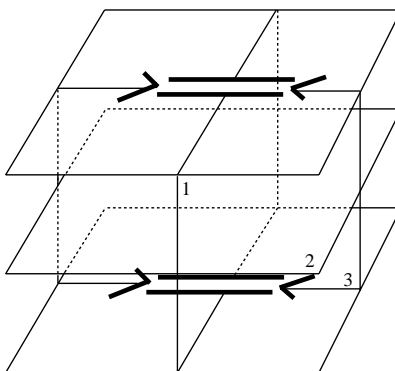


Figure 2: The maximum symmetry approach for ethylene is with relative motion only in plane 3. Then the orbitals in Fig. 3 can be defined first by their symmetry with respect to plane 1, and second by their symmetry with respect to plane 2. After Ref. 13.

The reaction that we consider here is the formation of cyclobutane from two molecules of ethylene, shown schematically in Fig. 1. This is the prototypical symmetry-forbidden reaction. Fig. 2 schematically depicts two ethylene molecules which we will describe with respect to the three planes shown. The two molecules are made to approach each other in the maximum-symmetry direction, namely with relative motion only in plane 3. We can then describe the π -bonding of the p orbitals with respect to planes 1 and 2, as well as the change in energy of the molecular orbitals with respect to the motion in plane 3. All of this information is contained in the correlation diagram of Fig. 3. The π and π^* on the left side of the figure indicate the π -bonding and π -antibonding molecular orbitals derived from

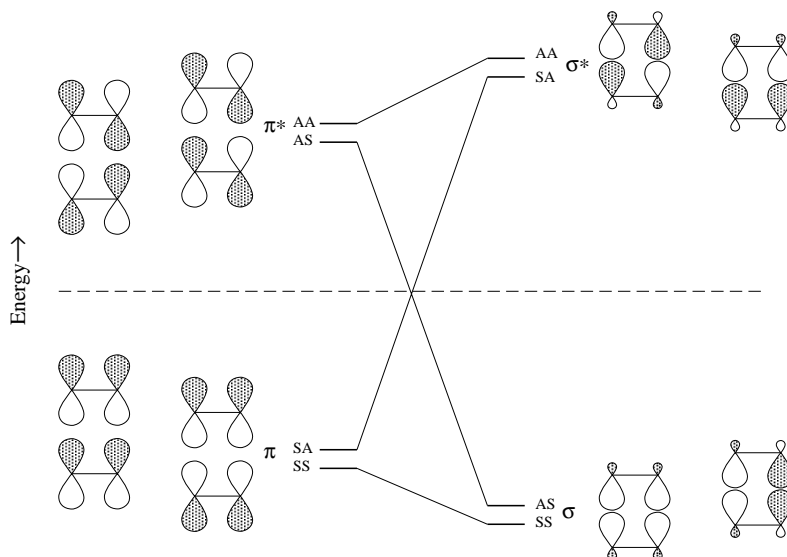


Figure 3: Correlation diagram for the maximum-symmetry approach of two ethylene molecules. The molecular orbitals below the dashed line are bonding orbitals, while the orbitals above the dashed line are antibonding orbitals. The orbitals are classified as symmetric or antisymmetric with respect to the planes defined in Fig. 2. After Ref. 13.

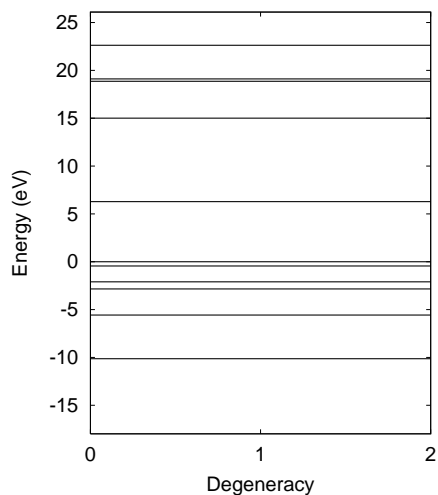


Figure 4: Molecular orbital energy level diagram for the two-ethylene system, before the molecules have come into contact, plotted with respect to the level degeneracy. The HOMO level has been set to the zero of energy. The orbitals are all two-fold degenerate, because there are two identical sets of orbitals, one associated with each ethylene.

the p atomic orbitals, which are extended in plane 3. The letters S and A indicate whether the molecular orbitals are symmetric or antisymmetric with respect to (first) plane 1 and (second) plane two. In the ground state, the molecular orbitals below the dashed line are occupied, whereas the molecular levels above this line are unoccupied. The movement in the energy levels is due to the interaction of the orbitals as they approach one another. On the right side of the figure, the p orbitals have become σ -bonded, as they would be in the cyclobutane molecule.

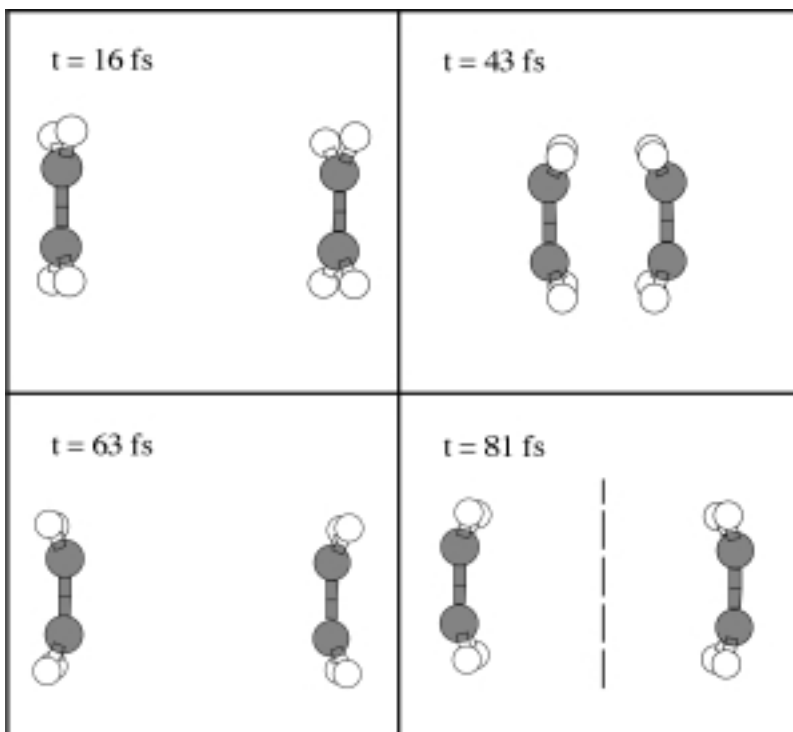


Figure 5: Snapshots of a simulation of two ethylene molecules approaching each other in the maximum-symmetry direction, with a kinetic energy of 0.2 eV. At $t = 43$ fs, the two ethylenes reach their closest point, with a separation of only 1.63 Å. However, they bounce off each other rather than bonding, and are 7.46 Å apart at $t = 81$ fs.

There are several interesting things to take note of in Fig. 3. First, the two energy levels are allowed to cross since they have different symmetry. Second, the occupied SA π -orbital on the left must move up in energy if we are to form molecular orbitals of cyclobutane on the right. Likewise, the AS π^* -orbital on the left will move down in energy to form the molecular orbital of cyclobutane. As a result of the motion, we are left with a molecule which has an unoccupied bonding state, as well as an occupied antibonding state. An estimate of the symmetry-imposed barrier for the face-to-face combination of two ethylene molecules is 5 eV. This is a significant barrier for thermal reactions, and indeed it is found experimentally that ethylene is very stable with respect to formation of cyclobutane.

Fig. 4 shows the ground state molecular orbital structure of the two ethylene molecules before they have come into contact. Notice that all of the levels are two-fold degenerate since

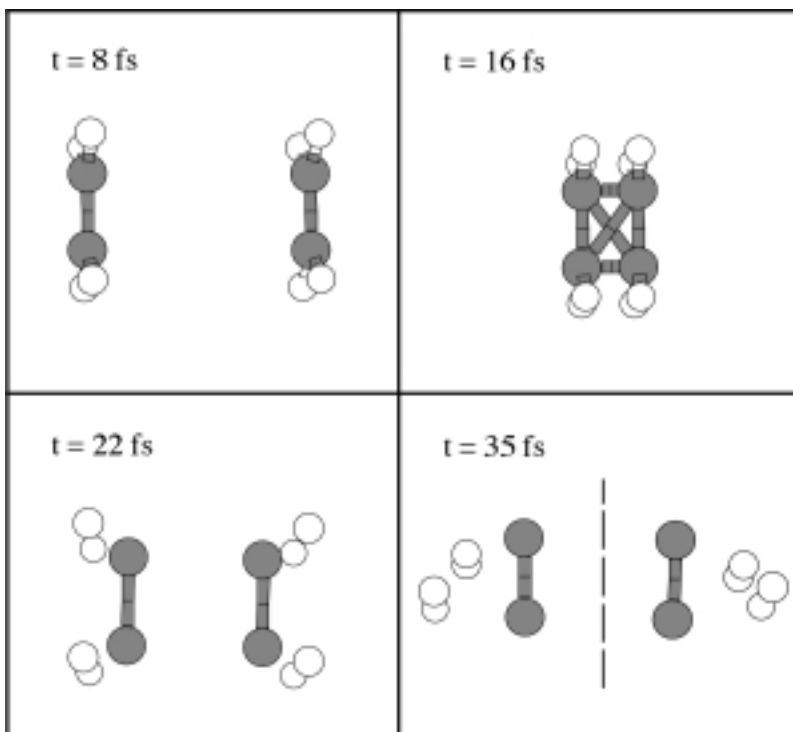


Figure 6: Snapshots of a simulation of two ethylene molecules approaching each other, in the maximum-symmetry direction, with a kinetic energy of 5.0 eV. At $t = 16$ fs, the ethylenes are within 0.95 \AA of each other, and then they violently bounce apart. The bonds shown between the two ethylenes at $t = 16$ fs are an artifact of the animation program used to make the snapshots, and do not represent true bonds.

we have two identical ethylenes. Fig. 5 shows snapshots of an animation of the interaction of two ethylenes, initially in the ground state, but given 0.2 eV of kinetic energy, put entirely into motion along the maximal-symmetry direction with zero impact parameter. At $t = 43$ fs, the two ethylene molecules reach their closest point of contact, with a separation of only 1.63 \AA . However, they do not bond, and instead simply bounce off each other. The dashed line in the snapshot at $t = 81$ fs is to indicate that the two molecules have moved out of the original field of view, and are 7.46 \AA apart.

In Fig. 6, the ethylenes were given 5.0 eV of kinetic energy along the maximal-symmetry direction. At $t = 16$ fs, the molecules are within 0.95 \AA of each other, but show no signs of bonding. (The bonds shown in the figure are artifacts of the animation program.) The ethylenes then violently recoil, and the carbon-hydrogen bonds are broken. At $t = 35$ fs the carbon atoms are 6.4 \AA apart.

On the other hand, if we first pump the electrons from the HOMO state to the LUMO state through the use of a properly-designed laser pulse, the reaction to form cyclobutane becomes energetically favorable as the two ethylenes approach each other in plane 3, allowing an occupied antibonding orbital to move down in energy to become a bonding orbital of cyclobutane, as well as letting an unoccupied bonding orbital move up in energy to become

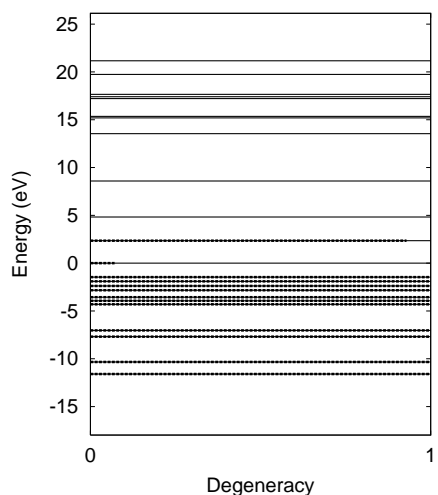


Figure 7: Molecular orbital energy-level diagram for the two-ethylene system following the irradiation of the ethylene on the right, in the $t = 56$ fs panel of Fig. 9, by a 5 fs FWHM, 5.5 eV laser pulse with a fluence of 1.4 KJ/m^2 . There has been almost a complete population inversion between the HOMO and LUMO levels. The occupied excited state has also moved down in energy. The HOMO level has been set to the zero of energy.

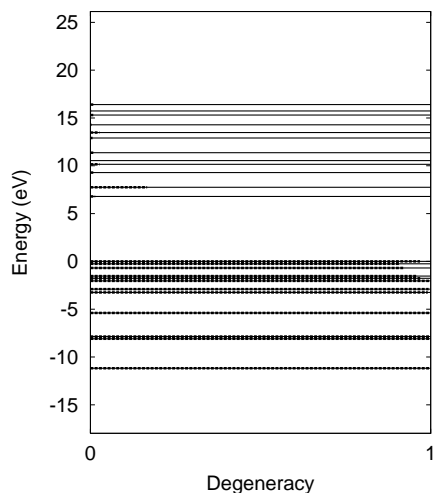


Figure 8: Molecular orbital energy-level diagram for the two-ethylene system of Fig. 7 at the end of 800 fs. The majority of the electrons once occupying the excited states have moved to the bonding states, and the HOMO-LUMO gap has increased once again, signifying the formation of a stable molecule. The HOMO level has been chosen as the zero of energy.

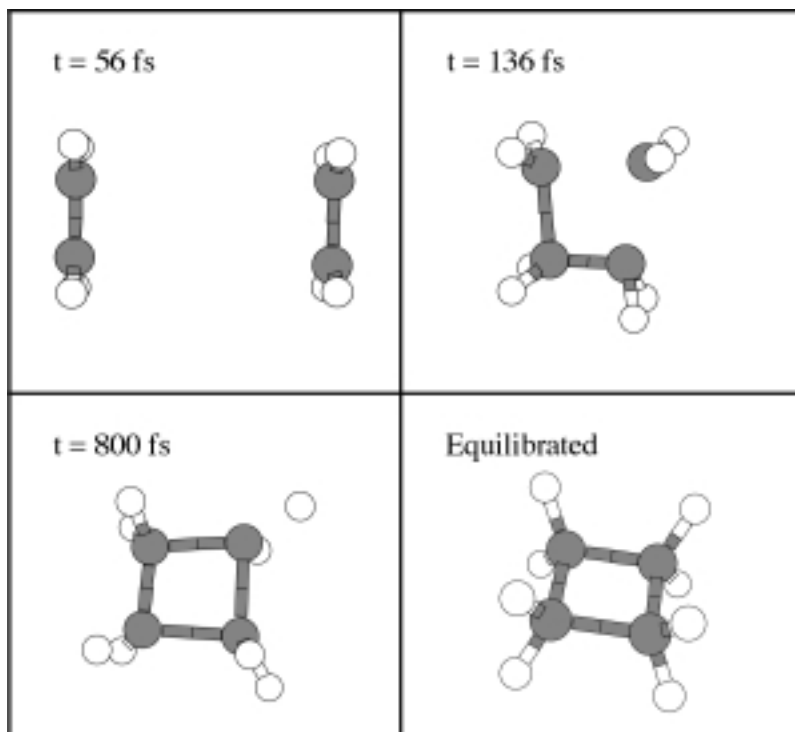


Figure 9: Snapshots of a simulation of the maximum-symmetry approach of two ethylene molecules following the irradiation of the ethylene on the right by a 5 fs FWHM, 5.5 eV laser pulse with a fluence of 1.4 KJ/m². The laser-pulse interaction with the ethylene molecule was sufficient to change the symmetry-forbidden reaction to one that is symmetry-allowed. In the bottom right panel, the structure has been equilibrated; all remaining electrons occupying excited states have been forced into the bonding states, and the excess kinetic energy has been removed.

an antibonding orbital of cyclobutane.

Fig. 7 shows the molecular orbital structure of the two-ethylene system, following the irradiation of the ethylene on the right (in the $t = 56$ fs panel of Fig. 9) by a 5 fs FWHM, 5.5 eV laser pulse with a fluence of 1.4 KJ/m². As a result of the pulse, Fig. 7 reveals that the HOMO level of the ethylene is nearly completely emptied, and that LUMO level is nearly completely filled. (The heavy dotted line over the molecular orbital indicates the degree to which the orbital is filled.) The LUMO level has also clearly moved down in energy. The formerly symmetry-forbidden reaction is now symmetry-allowed, leading to the formation of cyclobutane from two molecules of ethylene. Other results for this reaction are shown in Figs. 8 - 10. Fig. 8 shows the molecular orbital levels at the end of the simulation. Notice that there is still a small amount of electron occupancy in the excited states and that the HOMO-LUMO gap has once again opened up, signifying the formation of a stable structure. Fig. 9 consists of snapshots of the simulation, and Fig. 10 is a plot of the intermolecular separation of the two ethylenes as a function of time. In the panel on the lower right of Fig. 9, the cyclobutane molecule has been fully equilibrated. I.e, the kinetic energy has

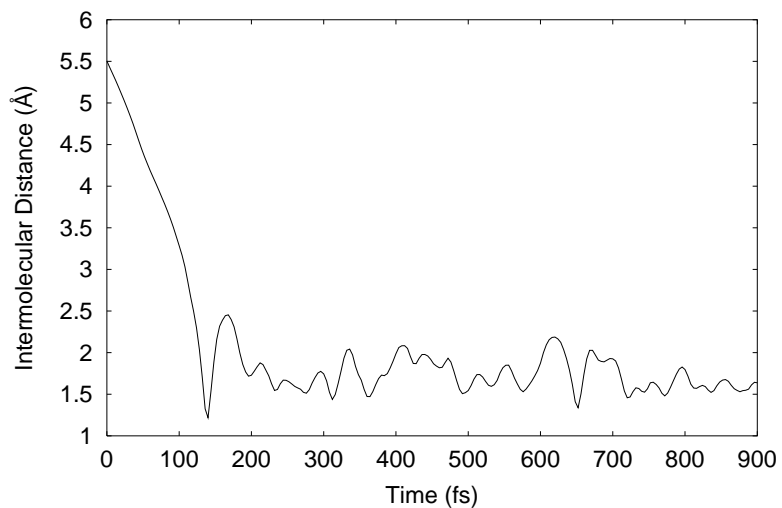


Figure 10: Intermolecular distance of the two-ethylene system plotted with respect to time, for the reaction in which the ethylene on the right (in the $t = 56$ fs panel of Fig. 9) has been excited by a 5 fs FWHM, 5.5 eV laser pulse with a fluence of 1.4 KJ/m^2 .

been removed, and all electrons remaining in antibonding states have been forced down to bonding states.

3 Photodissociation of Cyclobutane

The selective dissociation of cyclobutane, to form two molecules of ethylene, is also a very interesting and historically significant reaction. If we look back at the correlation diagram in Fig. 3, we can reverse the arguments that we used to understand the symmetry-forbidden nature of the reaction to form cyclobutane from two molecules of ethylene, to see that the dissociation of cyclobutane into two molecules of ethylene is also symmetry-forbidden. However, as in the previous simulation, if we promote electrons into the excited states with a laser pulse, the reaction can become symmetry-allowed. A question that arises, and that chemists have been investigating for the past 60 years both theoretically and experimentally, is the following: In what manner does the ring opening of cyclobutane to form two ethylene molecules occur? There are two possibilities. First, the reaction may proceed directly through a transition state at the saddle point of the activation barrier, as pictured schematically in Fig. 11, where the two σ -bonds in the cyclobutane ring break simultaneously to form two ethylene molecules. Calculations by Hoffmann et al. [14] indicated that the potential energy surface (PES) should be flat, allowing a transition state lifetime of ~ 40 fs.

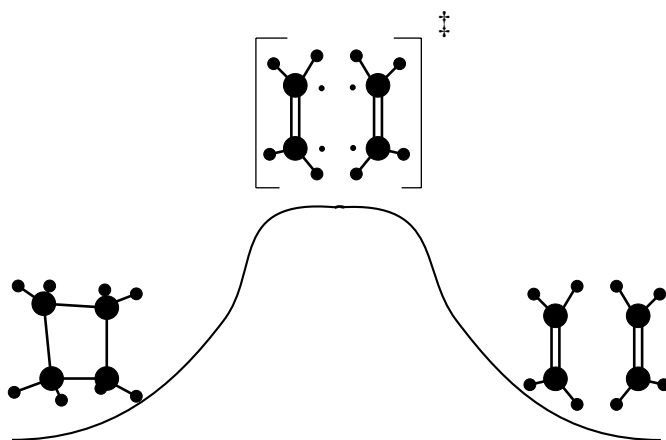


Figure 11: Schematic of the photodissociation reaction of cyclobutane to form two ethylene molecules. In this first scenario the cyclobutane molecule passes through a transition state in a concerted reaction, maintaining the original symmetry.

The second possibility is that the reaction proceeds through a two-step process, with one of the σ -bonds first breaking to form tetramethylene as a diradical reaction intermediate, which then passes through a transition state to yield the final products. This possibility is pictured in Fig. 12. The diradical mechanism is important because the concept of diradicals as intermediates has been hypothesized to be the prototype of chemical bond transformations in many classes of thermally activated and photochemical reactions. The question of which path the reaction follows is crucial in understanding the fundamental nature of the reaction dynamics: a concerted one-step process, or a nonconcerted two-step process.

Theorists have not been able to produce a definitive answer to this problem. However, the ground-breaking work of the Zewail group (one of the five discoveries cited in the an-

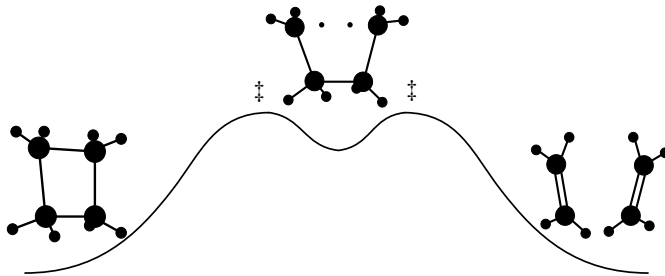


Figure 12: Schematic of the photodissociation reaction of cyclobutane to form two ethylene molecules. In this second scenario the cyclobutane molecule first forms the tetramethylene diradical reaction intermediate, before transitioning to the final state of two ethylene molecules.

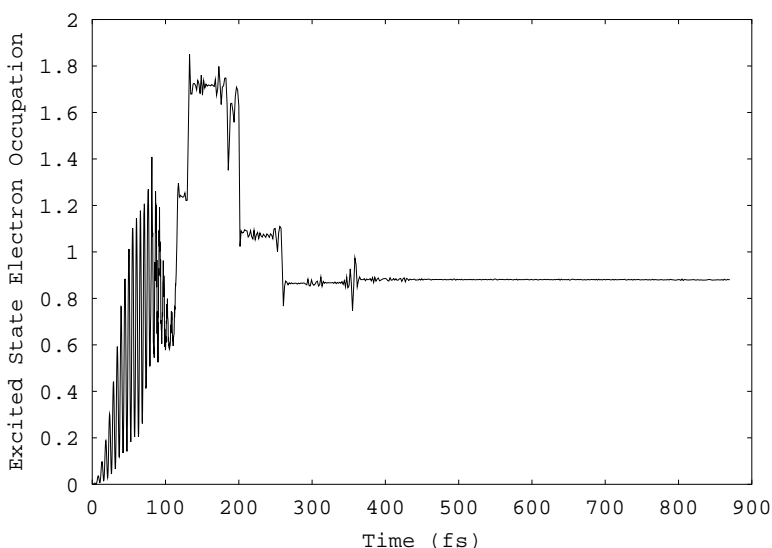


Figure 13: Excited state electron occupancy plotted as a function of time, for a cyclobutane molecule irradiated by a 60 fs FWHM laser pulse, centered at 6.5 eV, with a fluence of 42.21 KJ/m². The electrons are mainly excited by a two-photon process until about 110 fs, where a one-photon process becomes possible because the excited-state energies have decreased.

nouncement of Ahmed Zewail's receiving the 1999 Nobel Prize in Chemistry) showed that the reaction proceeded through the two-step process [15]: first forming the tetramethylene diradical, and then proceeding to the products. They were able to control the lifetime of the reaction intermediate from 340 fs to 700 fs by adjusting the fluence of the pump pulse from a 60 fs FWHM laser, using a two-photon process.

To photodissociate cyclobutane in our simulations, via a two-photon process, we used a 60 fs FWHM laser pulse, centered at 6.5 eV, with a fluence of 42.21 KJ/m². Fig. 13 shows the number of electrons occupying the excited states as a function of time. Notice the rapid

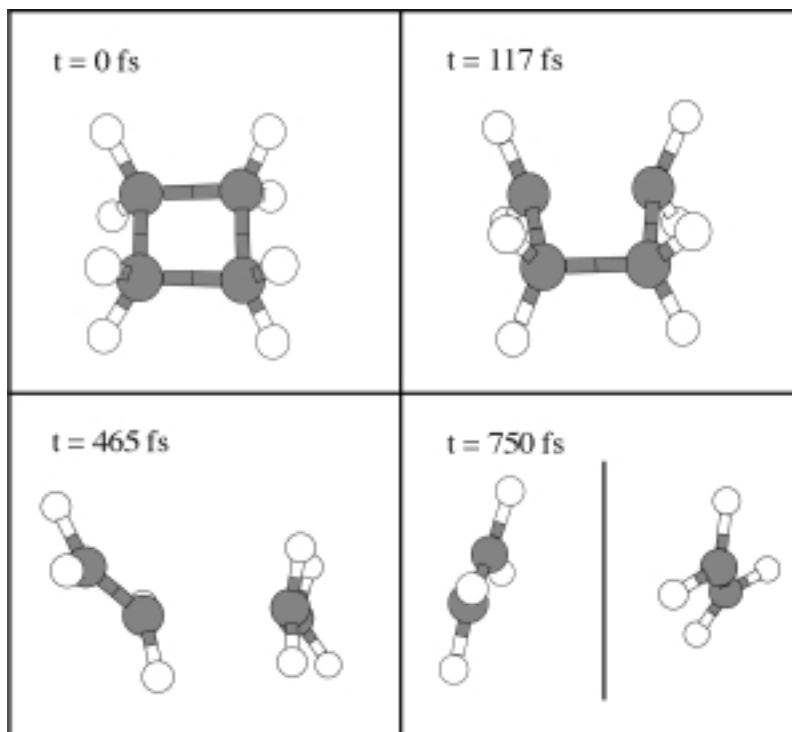


Figure 14: Snapshots of a simulation of the photodissociation of cyclobutane to form two ethylene molecules. The cyclobutane molecule was irradiated by a 60 fs FWHM laser pulse, centered at 6.5 eV, with a fluence of 42.21 KJ/m². The formation of the tetramethylene diradical reaction intermediate appears at about $t = 117$ fs. At $t = 465$ fs, the diradical makes a transition to the final products: two ethylenes which are seen to be stable at $t = 750$ fs. The vertical bar in the bottom-right panel indicates that the two ethylene molecules are no longer contained in the original field of view.

oscillations that occur during the first 110 fs of the pulse, where the absorption is dominated by a two-photon process. During the final 10 fs of the pulse (which has a total duration of 120 fs for the pulse shape used in these simulations [5, 6]), the excited-state molecular orbitals have moved down in energy, leading to very rapid absorption that can now occur through a one-photon process. This is accompanied by breaking of a σ -bond, which produces the tetramethylene diradical reaction intermediate, as can be seen in the top-right panel of Fig. 14 where snapshots from the simulation are shown. At the end of the pulse, about 1.25 electrons occupy the excited states. Soon after the pulse the occupancy of excited states is increased by about 0.25 electrons; this is associated with a rapid conversion of kinetic energy to effective potential energy, as can be seen in the plot of kinetic energy with respect to time in Fig. 15. Near 200 fs, approximately 0.8 electrons rapidly fall back into bonding states. Fig. 16 shows the occupation of excited states with respect to time between 195 fs and 205 fs. Notice that the depopulation of excited states occurs in less than 2 fs. It is characteristic of barrierless electronic transitions that they can occur in time intervals which are of the order of a few cycles of the characteristic frequency – which is less than 1 fs for 6.5 eV radiation.

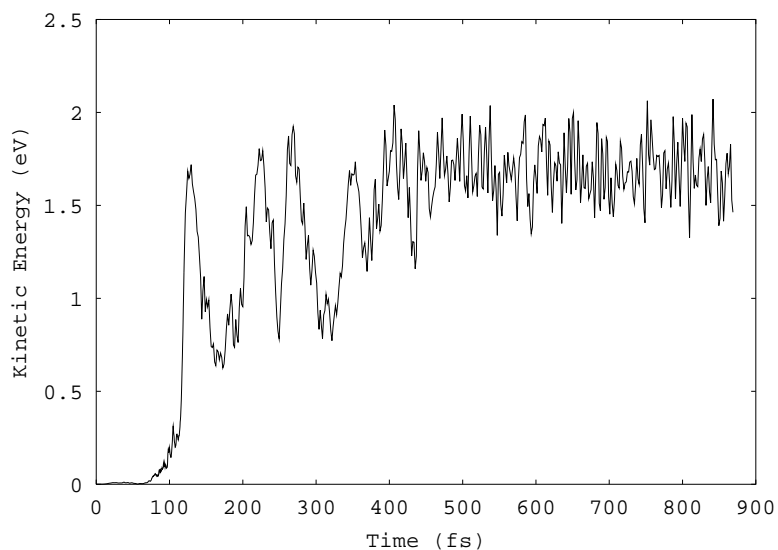


Figure 15: Kinetic energy plotted as a function of time for a cyclobutane molecule irradiated by a 60 fs FWHM laser pulse, centered at 6.5 eV, with a fluence of 42.21 KJ/m².

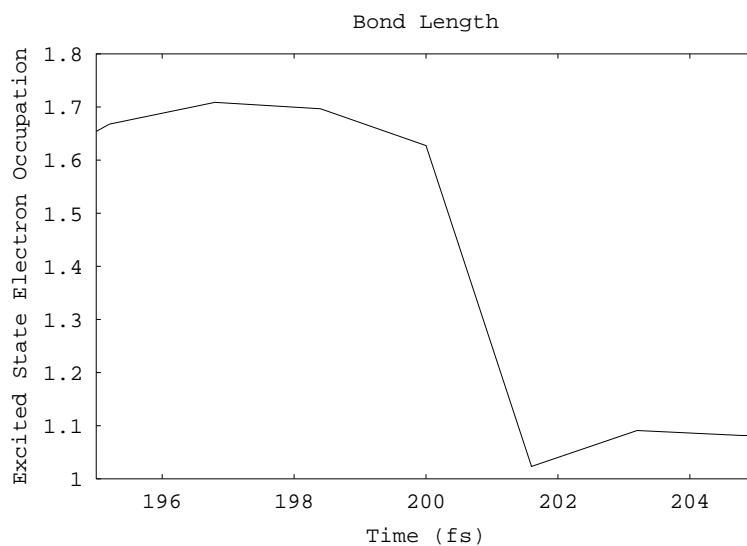


Figure 16: A portion of Fig. 13 shown in more detail to exhibit the time scale for the rapid transition near 200 fs. This transition occurs on a time scale comparable to a few periods of the radiation field, indicating that it is a barrierless transition.

The diradical passes through its transition state at ~ 465 fs, with the appearance of two ethylene molecules. Fig. 17 is a plot of the carbon-carbon interatomic bondlength for the two carbons on the left side of the cyclobutane molecule in the top-left panel of Fig. 14. At

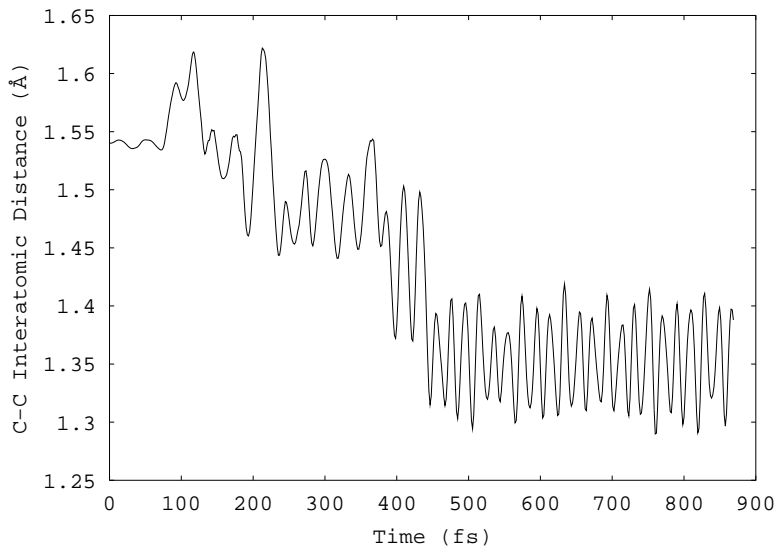


Figure 17: Plot of the carbon-carbon interatomic bondlength for the two carbons making up the left side of the cyclobutane molecule (in the top-left panel of Fig. 14). At $t = 0$, the value for the bondlength is 1.54 Å, characteristic of cyclobutane. After the passage through two transition states, we see that the value finally begins oscillating around 1.35 Å, which is characteristic of the carbon-carbon bondlength in ethylene.

$t = 0$, the value for the bondlength is 1.54 Å, which is characteristic of cyclobutane. After the passage through two transition states, we see that the value of the bondlength finally begins oscillating around 1.35 Å, which is characteristic of the carbon-carbon bondlength in ethylene. Our simulation thus yields a lifetime for the reaction intermediate of approximately 348 fs, in good agreement with the experiments discussed above.

We never obtained a lifetime longer than 348 fs in our simulations. However, we were able to obtain shorter lifetimes by increasing the pump fluence by only $9.6 \times 10^{-3}\%$. The results of this simulation are shown in Figs 18-21. The lifetime of the reaction intermediate in this case was approximately 197 fs. If we increased the fluence further, hydrogen atoms were ejected from the cyclobutane molecule, leading to very different dynamics.

The ability to correctly describe the photodissociation of cyclobutane, as demonstrated in these last two simulations, is a surprising triumph for DFTED. To accurately describe the excited-state energy surface for a complex system, with 30 vibrational degrees of freedom and 24 valence electrons, represents a highly nontrivial level of success.

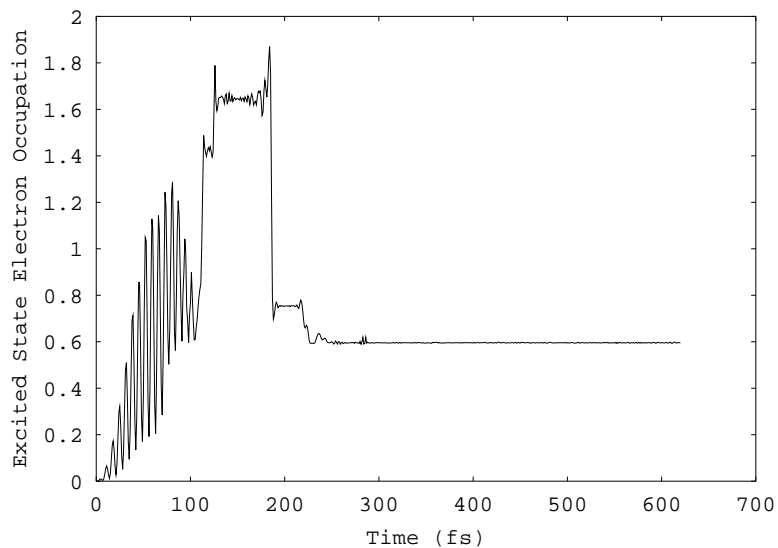


Figure 18: Excited-state electron occupancy plotted as a function of time for a cyclobutane molecule irradiated by a 60 fs FWHM laser pulse, centered at 6.5 eV, with an increase in the pump fluence of only $9.6 \times 10^{-3}\%$ compared to the simulation of Fig. 13. The electrons are found to be excited by a two-photon process until 110 fs, where they are then excited through a one-photon process. (Since the full-width-at-half-maximum duration of the pulse is 60 fs, the total duration is 120 fs for the pulse shape used in the present simulations [5, 6].)

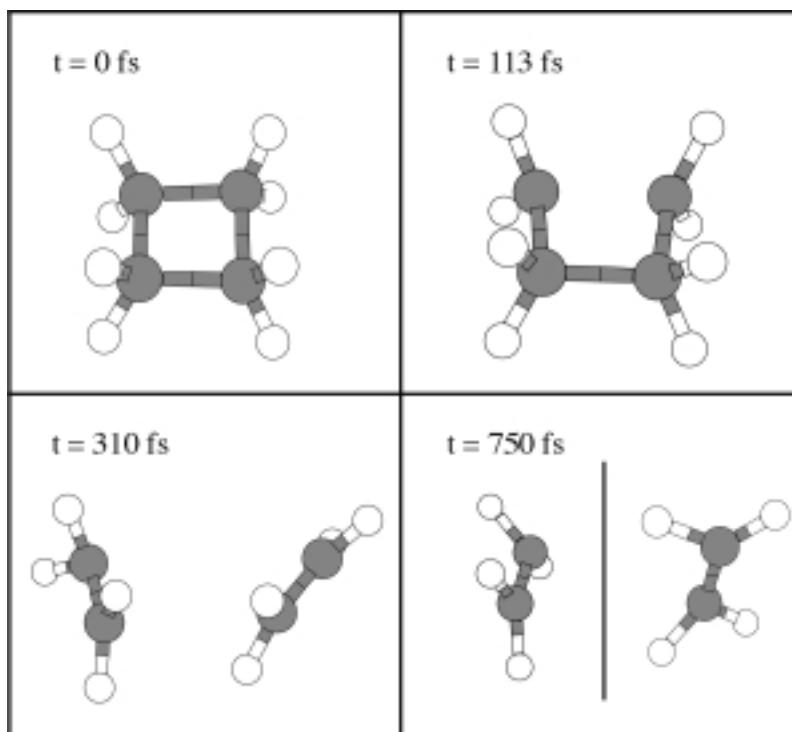


Figure 19: Snapshots of a simulation of the photodissociation of cyclobutane to form two ethylene molecules. The cyclobutane molecule was irradiated by a 60 fs FWHM laser pulse, centered at 6.5 eV, with an increase in pump fluence of only $9.6 \times 10^{-3}\%$ compared to the simulation in Fig. 13. The formation of the tetramethylene diradical reaction intermediate appears at about $t = 113$ fs. At $t = 310$ fs, the diradical undergoes a transition to the final products: two ethylenes which are seen to be stable at $t = 750$ fs. The vertical bar in the bottom-right panel indicates that these ethylene molecules are no longer contained in the original field of view.

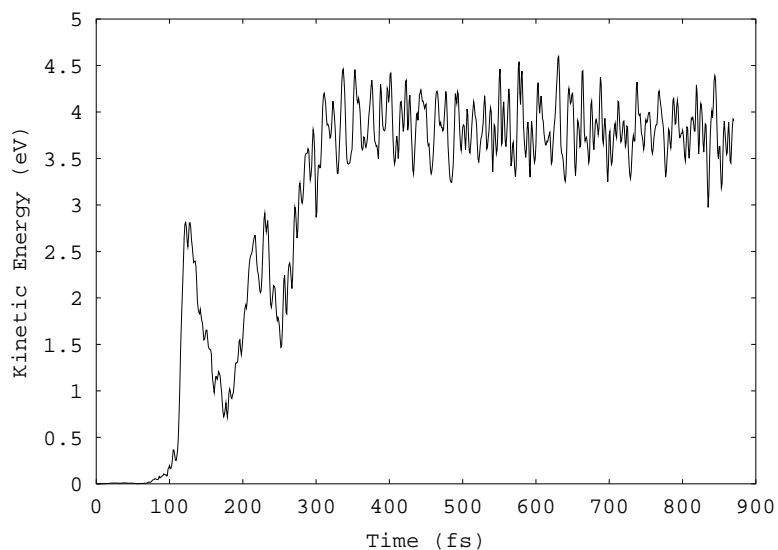


Figure 20: Kinetic energy plotted as a function of time for a cyclobutane molecule irradiated by a 60 fs FWHM laser pulse, centered at 6.5 eV, with an increase in the pump fluence of $9.6 \times 10^{-3}\%$ compared to the simulation in Fig. 13.

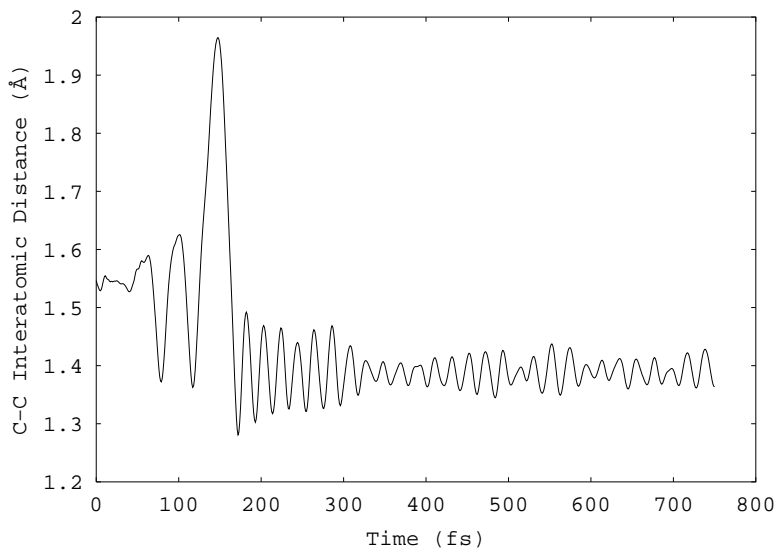


Figure 21: Plot of the carbon-carbon interatomic bondlength of the two carbons making up the left side of the cyclobutane molecule (in the top-left panel of Fig. 19). At $t = 0$ fs, the value for the bondlength is 1.54 Å, characteristic of cyclobutane. After the passage through two transition states at 310 fs, we see that the value finally begins oscillating around 1.35 Å, which is characteristic of the carbon-carbon bondlength in ethylene.

4 Photoisomerization of Butadiene

Isomerization reactions are an important class of chemical reactions. They involve the change of a molecule from one conformation to another. One of the most important and most fascinating is the cis-to-trans photoisomerization of retinal, the chromophore in rhodopsin. This is the primary event in the process of vision. It has been recently shown in the beautiful pump-probe experiments of Mathies and co-workers to occur in only 200 fs [16, 17].

The complexity of the retinal molecule, together with the complexity of the protein environment provided by rhodopsin, makes a simulation of the photoisomerization of retinal challenging enough to be a multiyear project for the future. Here, however, we will investigate the photoisomerization of butadiene, which is a simpler but analogous photoinduced conformational change schematically depicted in Fig. 22. This reaction has experimentally been shown to proceed in both directions by Müller et al. [18], using continuous incoherent light centered at 5.8 eV to stimulate the trans-to-cis photoisomerization reaction, and 5.5 eV light to stimulate the cis-to-trans reaction. It is also known that trans-butadiene is more stable by approximately 0.1 eV than cis-butadiene. Our model underestimates this difference in energy by about 1/2, but trans-butadiene is still the more stable of the two conformers. A schematic representation of the experiment which we wish to simulate is shown in Fig. 23. In this figure, butadiene in the trans conformer is photoexcited to an excited-state potential energy surface (PES) which drives the molecule toward the cis conformation. The nearness of the minimum of the excited-state PES and the saddle point of the ground state PES allows for efficient nonradiative transitions to the cis conformation. The excited-state PES is shown as nearly symmetric with respect to the trans and cis sides of the isomerization coordinate, to indicate that the dynamics of the reverse reaction from cis-to-trans should proceed in a similar fashion and on a similar time scale.

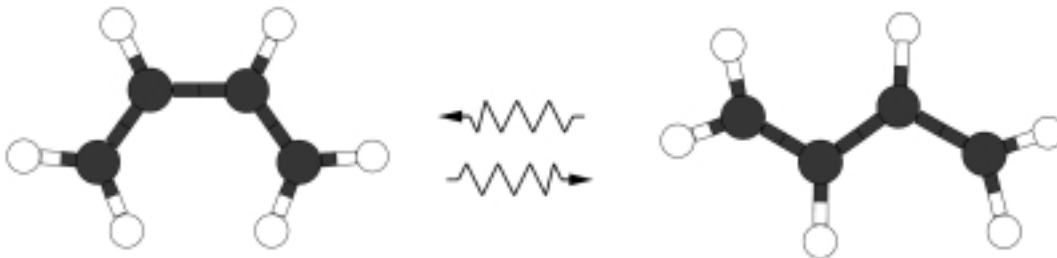


Figure 22: Schematic of the photoinduced structural changes that occur in the photoisomerization reaction of butadiene.

5 Trans-to-Cis Photoisomerization of Butadiene

Snapshots of a simulation for the photoisomerization reaction of trans-butadiene are shown in Fig. 24. The laser pulse used to facilitate the reaction had a FWHM pulse duration of 75 fs, was centered around 4.18 eV, and had a fluence of 0.76 KJ/m². A plot of the electron

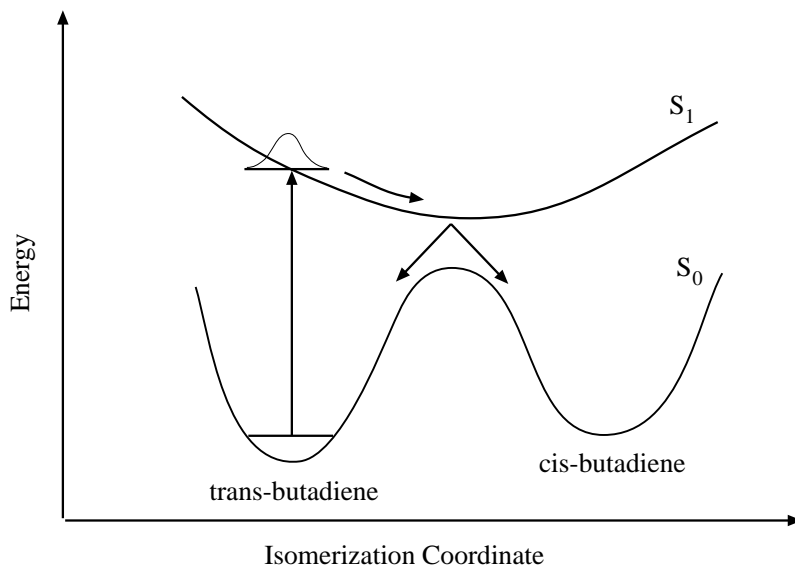


Figure 23: Schematic diagram of butadiene in the trans conformer, photoexcited to an excited-state potential energy surface (PES) which drives the molecule towards the cis conformation. The nearness of the minimum of the excited-state PES to the saddle point of the ground-state PES allows for efficient nonradiative transitions to the cis conformation. The excited-state PES is shown as nearly symmetric with respect to the trans and cis sides of the isomerization coordinate, to imply that the dynamics of the reverse reaction from cis-to-trans should proceed in a similar fashion and on a similar time scale.

occupancy of the excited states as a function of time is shown in Fig. 25. It is interesting to note the step-like behavior in the occupancy, as the electrons nonradiatively fall back to the bonding orbitals after the pulse has been completed (at 150 fs, since the total pulse duration is twice the FWHM duration). These downward steps in electron occupation of the excited states are associated with rotation of the two outer carbons about their respective double bonds, as can be seen for the outer carbon on the right in the top-right panel of Fig. 24. From a molecular-orbital point of view, this rotation acts to mix the excited-state and ground-state molecular orbitals of butadiene. The drop in the occupancy of the excited-state orbitals is also evident in the plot of the kinetic energy with respect to time in Fig. 26. By $t = 250$ fs, the electron occupancy has stabilized and the motion of the molecule is highly kinetic. However, the motion is within an overall trans-butadiene conformer until, at 530 fs, there is dramatically different motion about the single bond joining the two middle carbon atoms, as can be seen in the bottom left panel of Fig. 24. At this point we observe the sudden emergence of the cis conformation. Although the motion is still highly kinetic, there is now no manifestation of the trans conformation. This transformation is very clearly apparent in the plot of Fig. 27 showing the bondlength for the two outside carbon atoms, which has a value of about 3.7 Å for trans and 3.1 Å for cis. The last thing to note is that the dramatic rotation about the single bond, which signaled the onset of the cis conformer, did not produce a change in the electron occupancy, shown in Fig. 25. This feature can be

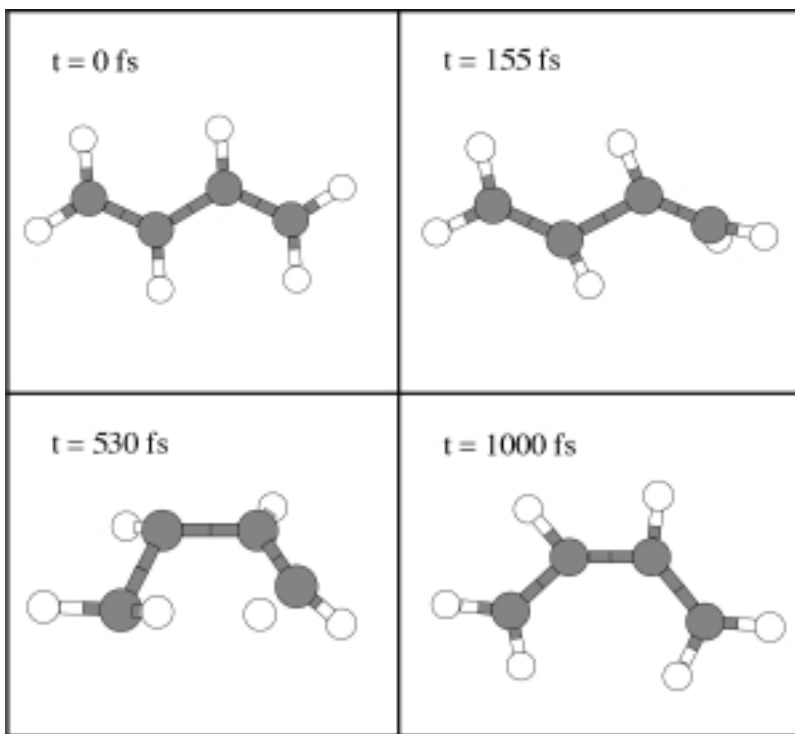


Figure 24: Snapshots of the photoisomerization reaction of trans-butadiene induced by a laser pulse of duration 75 fs FWHM, centered at 4.18 eV and having a fluence of 0.76 KJ/m². At $t = 155$ fs, the carbon on the left of the structure rotates about its carbon-carbon double bond. At $t = 530$ fs, the middle carbon atoms rotate about their single bond, leading to the formation of cis-butadiene. The entire reaction takes place in 550 fs.

understood if we consider a rotation about the single bond joining the two middle carbon atoms in Fig. 28, and its effect on the π -orbitals. This type of rotation does not mix the bonding and antibonding states.

6 Cis-to-Trans Photoisomerization of Butadiene

To investigate the reverse reaction, the photoisomerization of cis-butadiene, we irradiated this molecule with a 75 fs FWHM, 4.15 eV laser pulse, having a fluence of 1.3 KJ/m². The results are shown in Figs. 29 - 32, and they demonstrate that the reaction can indeed proceed in both directions, as was found experimentally. Fig. 29 also shows the step-like behavior as the electrons occupying the excited states nonradiatively fall back to the bonding states. The large drop in excited-state occupancy is correlated with a very efficient simultaneous rotation of both outer carbon atoms, as shown in the upper right panel of Fig. 32. The rotation about the single bond in this reaction occurs at 519 fs. Just as before, it signals a change in conformation, after which we see only the trans conformer.

The striking similarities between the two reactions appear to validate the hypothesis that

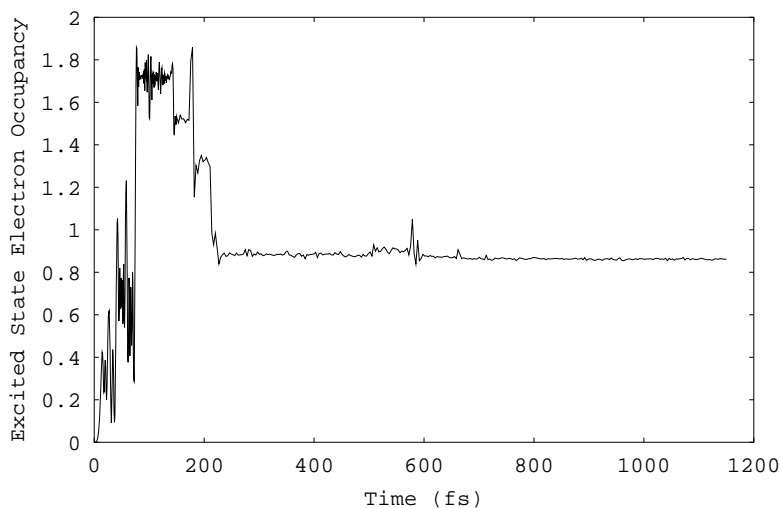


Figure 25: Plot of the occupation of the antibonding states as a function of time during the photoisomerization reaction of trans-butadiene induced by a laser pulse with a duration of 75 fs FWHM, centered at 4.18 eV and having a fluence of 0.76 KJ/m².

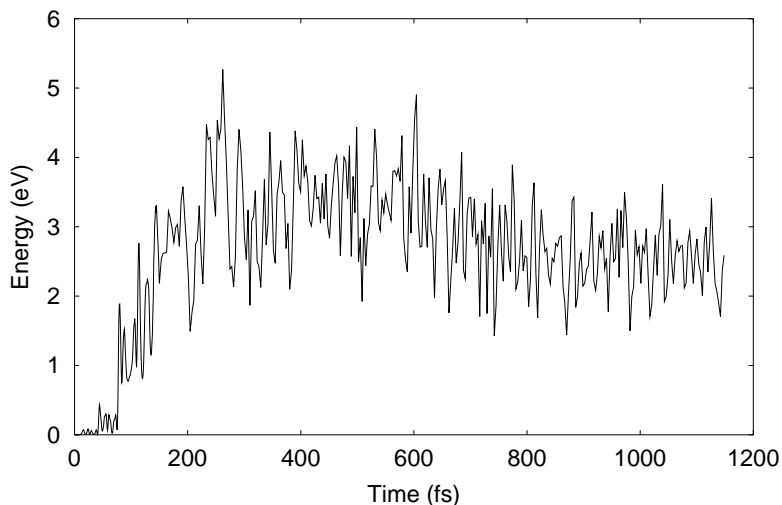


Figure 26: Kinetic energy plotted as a function of time during the photoisomerization reaction of trans-butadiene induced by a laser pulse with a duration of 75 fs FWHM, a photon energy of 4.18 eV, and a fluence of 0.76 KJ/m².

the excited state PES is nearly symmetric with respect to the two potential wells along the reaction coordinate.

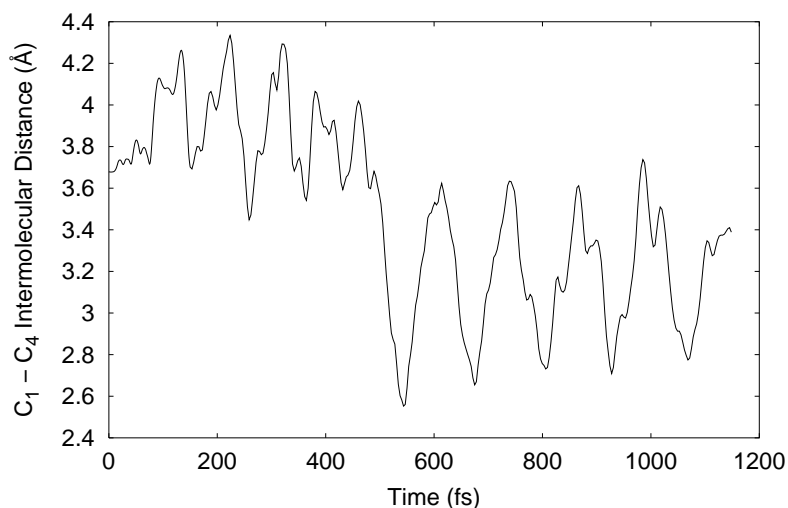


Figure 27: Carbon-carbon bondlength for the carbon atoms on the ends of a butadiene molecule, plotted as a function of time during the photoisomerization reaction of trans-butadiene, induced by a laser pulse with a duration of 75 fs, a photon energy of 4.18 eV, and a fluence of 0.76 KJ/m². The characteristic bondlength for trans-butadiene is about 3.7 Å, and that for cis-butadiene is 3.1 Å.

The remarkable success of the above simulations for butadiene offers the promise that we will be able, at some point in the future, to simulate a complex biological process like the photoisomerization of retinal.

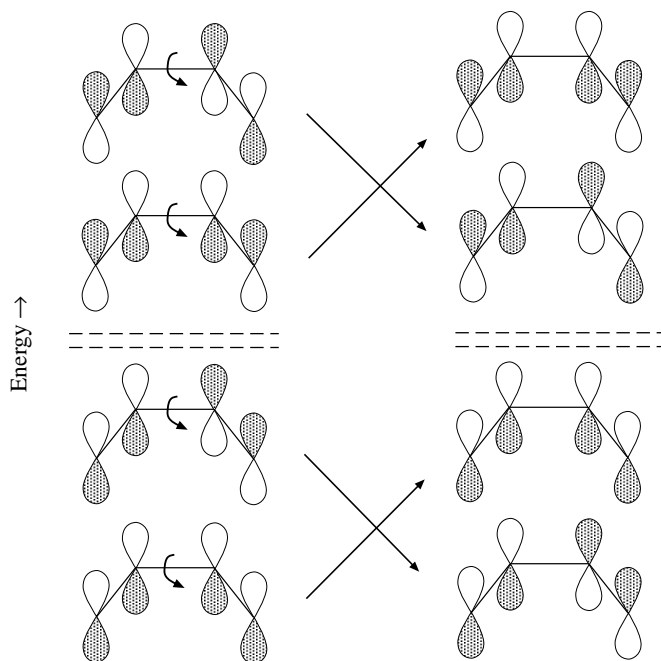


Figure 28: The π -orbitals of butadiene, and how they transform with respect to a 180 degree rotation about the single bond – i.e., the bond connecting the two inner carbon atoms.

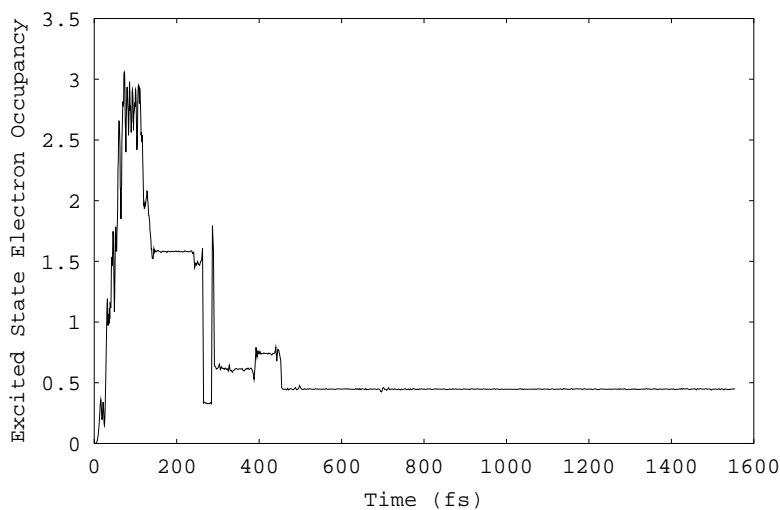


Figure 29: Occupation of the antibonding states as a function of time during the photoisomerization reaction of cis-butadiene induced by a laser pulse of duration 75 fs, photon energy of 4.15 eV, and fluence of 1.3 KJ/m².

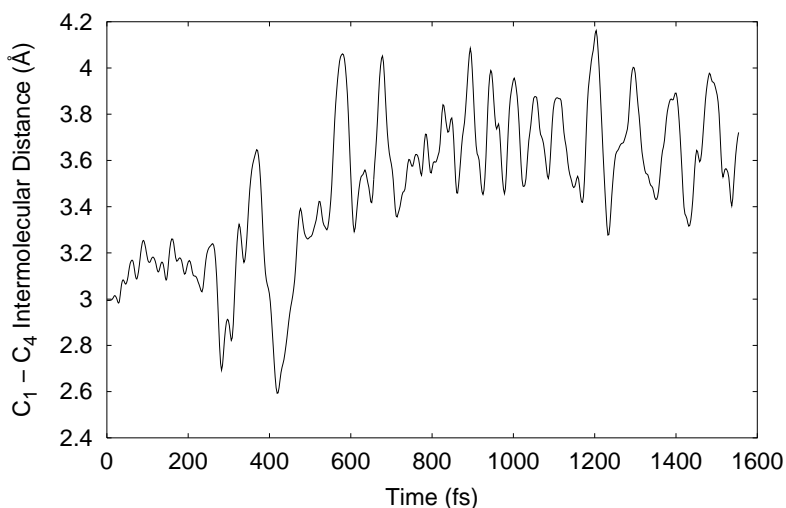


Figure 30: Carbon-carbon bondlength for the carbon atoms on the ends of the butadiene molecule, plotted as a function of time during the photoisomerization reaction of cis-butadiene, induced by a laser pulse with a duration of 75 fs, photon energy of 4.15 eV, and fluence of 1.3 KJ/m². The characteristic bondlength for cis-butadiene is 3.1 Å. The characteristic bondlength for trans-butadiene is 3.7 Å.

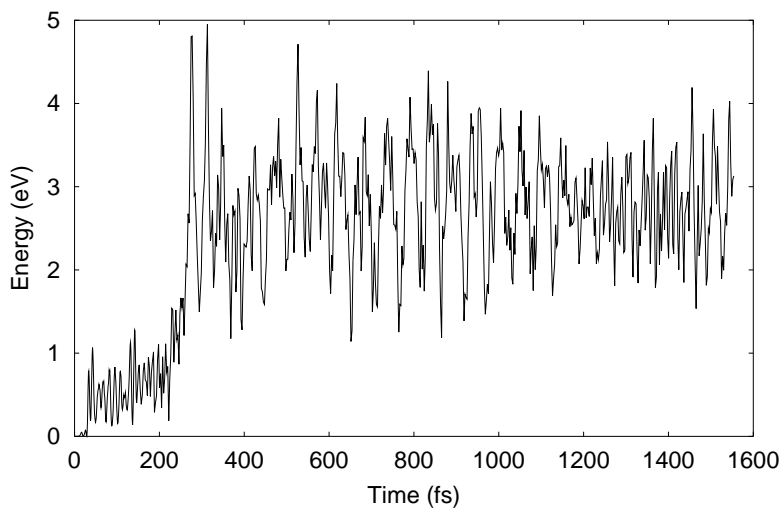


Figure 31: Kinetic energy plotted as a function of time during the photoisomerization reaction of cis-butadiene induced by a laser pulse of duration 75 fs, photon energy 4.15 eV, and fluence 1.3 KJ/m². Notice the sharp increase of kinetic energy at $t = 248$ fs.

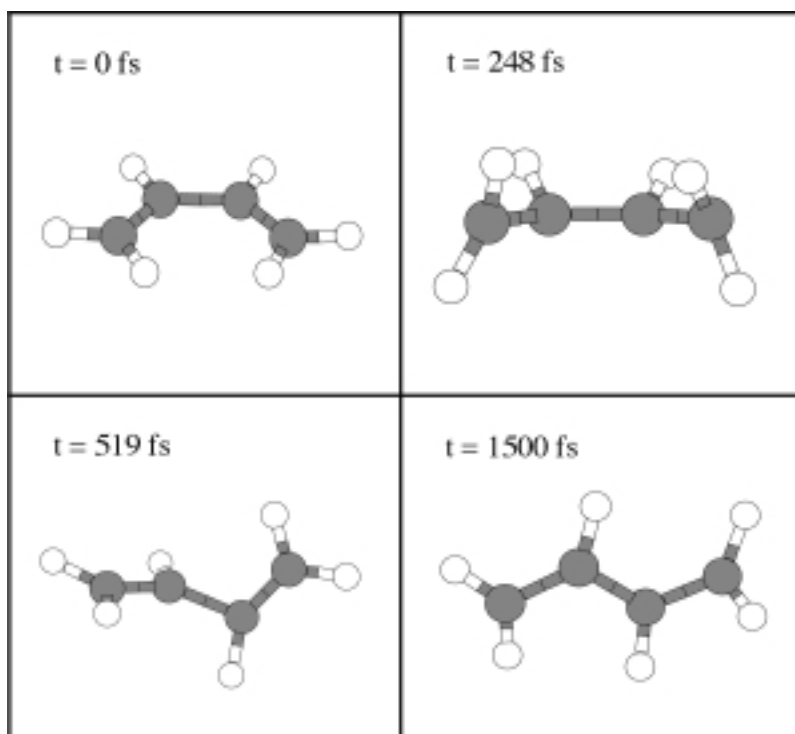


Figure 32: Snapshots of the photoisomerization reaction of cis-butadiene induced by a laser pulse of duration 75 fs, photon energy 4.15 eV, and fluence 1.3 KJ/m². At $t = 248$ fs, both carbons on the ends rotate about the carbon-carbon double bonds. At $t = 519$ fs, the structure rotates about the single bond connecting the middle carbon atoms, leading to the formation of trans-butadiene. The entire reaction takes place in 650 fs.

7 Two-Pulse Coherent Control of Benzene

Advances in laser technology have stimulated new interest in the goal of harnessing interference phenomena— inherent in the interaction between light and matter, as well as in the quantum behavior of electrons and nuclei— to drive a chemical system to a desired final state. Experimentally, progress has been made in the control of vibrational modes in materials [19], the creation and destruction of excitons in semiconductor quantum wells [20], the ground-state rotational coherence of linear molecules [21], and the femtosecond-scale chemical reactions of small molecules [22]. Theoretical investigations have relied on linear-response theory to solve the Liouville equation [23, 24], or direct solution of the Schrödinger equation [25, 26]. In contrast to such one-photon theoretical approaches, multi-photon control schemes have been developed and utilized in experiments [27, 28]. A theoretical scheme that includes higher-order processes is therefore needed for comparison with the available experimental data, as well as for understanding future experiments in this evolving frontier of science.

Using linear response theory, Shapiro [25] showed that the effect of a short laser pulse on the coefficient of some final state of a quantum system is given by

$$c_f(t) = -(\mu_{fi}/i\hbar) \int_{-\infty}^t dt' \exp(i\omega_{fi}t') \varepsilon(t'), \quad (1)$$

where

$$\mu_{fi} = \langle \psi_f | \mu | \psi_i \rangle \quad (2)$$

is the dipole-moment matrix element for the transition from the initial to the final state, $\varepsilon(t')$ is the electric field of the laser pulse, and $\omega_{fi} = \omega_f - \omega_i$. He then showed that

$$c_f(\infty) = (2\pi i/\hbar) \mu_{fi} \tilde{\varepsilon}(\omega_{fi}) \quad (3)$$

where $\tilde{\varepsilon}$ is the Fourier transform of the pulse. He further argued that, since no transitions are possible after the completion of the pulse, the infinite-time condition should be established soon after the completion of the pulse, provided that the pulse is short with respect to other processes in the system. Since the coefficients now contain resonant-frequency information from the pulse, a second pulse properly delayed in time and phase can lead to interference effects which can be used to control the outcome for the system.

In our simulations, we explore coherent control of both the electronic excitations and the atomic vibrations, via a pump-pulse, control-pulse sequence applied to benzene. The choice of benzene allows us to continue our work with organic molecules, as well as demonstrate coherent control of a complex system containing 30 valence electrons and 30 vibrational degrees of freedom.

An equilibrated benzene molecule is shown in Fig. 33. We will be primarily interested in the two fully-symmetric vibrational modes of this molecule: In the breathing mode, the carbon and hydrogen atoms move radially together in the plane of the molecule; whereas the beating mode involves radial motion of the carbons and hydrogens in opposite directions.

Before we examine the response of benzene to a pump-pulse, control-pulse sequence, let us first consider the response to a single 10 fs FWHM, 5.2 eV pump pulse with a fluence of 3.0×10^{-3} KJ/m². The effect on the occupation of excited states is shown in Fig. 34.



Figure 33: Benzene molecule in the ground state. It has two fully-symmetric vibrational modes: In the breathing mode, the carbon and hydrogen atoms move radially together in the plane of the molecule; in the beating mode they also move radially, but in opposite directions.

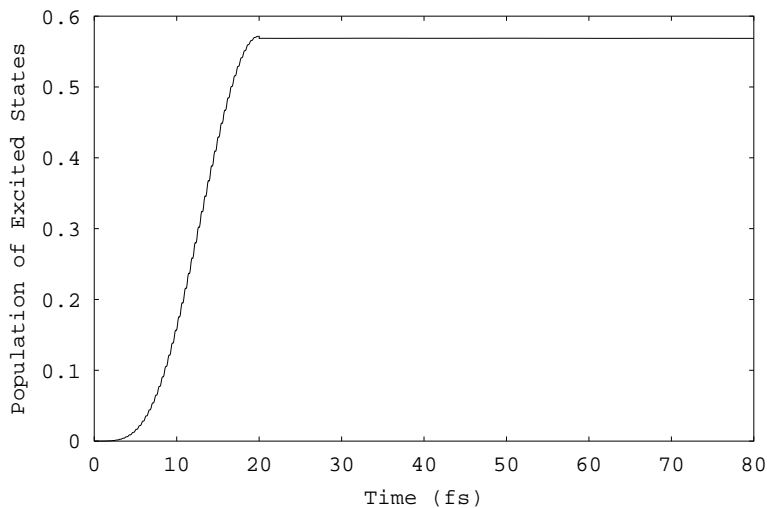


Figure 34: Population of electrons in excited states, plotted as a function of time following a 10 fs FWHM pump laser pulse, centered at 5.2 eV, with a fluence of 3.0×10^{-3} KJ/m².

The HOMO-LUMO gap of benzene in our model is 5.14 eV, so we see the excited states being filled in a typical one-photon resonant process. After the completion of the pulse at 20 fs, the occupation is constant, with $\sim 2\%$ of the electrons occupying the excited states for the remaining picosecond of the simulation. This indicates that there are no appreciable nonradiative processes in benzene at this fluence, and that benzene is stable with this level of occupation of the excited states. Fig. 35 shows the Fourier power spectrum for a subsequent one picosecond simulation, following the laser pulse described above. The spectrum is dom-

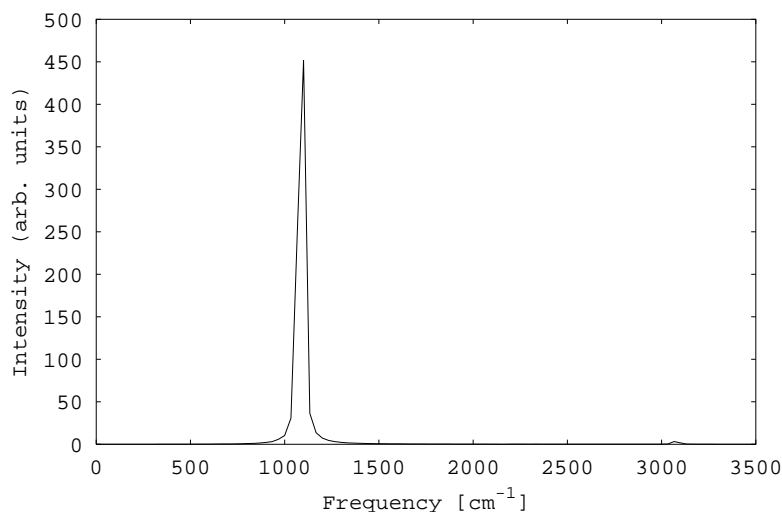


Figure 35: Fourier power spectrum of benzene for a picosecond run following a 10 fs FWHM pump laser pulse, centered at 5.2 eV, with a fluence of 3.0×10^{-3} KJ/m². The breathing mode at 1100 cm⁻¹ is dominant.

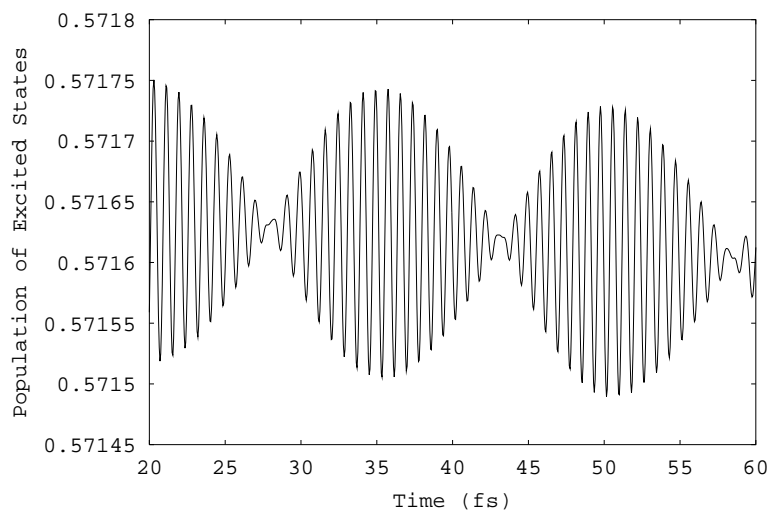


Figure 36: A close-up view of Fig. 34, for 40 fs following the completion of the pump pulse. The structure in the excited-state occupancy is composed primarily of two frequency components. One has a period of 0.8 fs, which corresponds to the frequency of the external field. The other has a period of 31.2 fs, which corresponds to the frequency of the breathing-mode vibration.

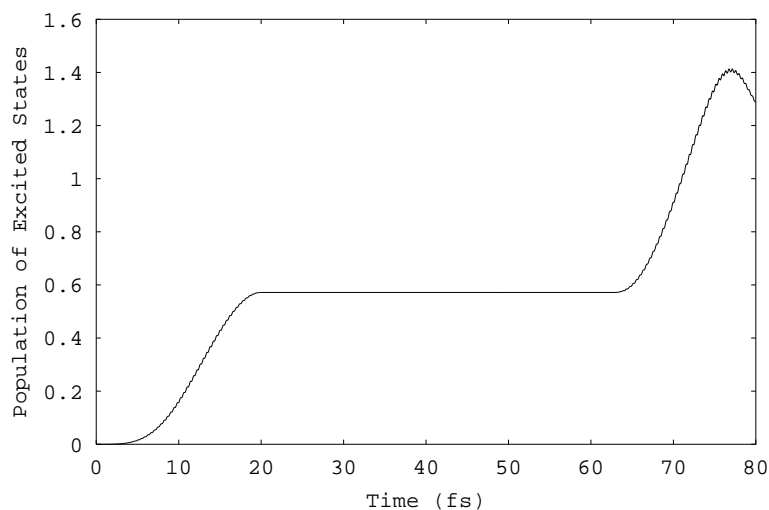


Figure 37: Population of the excited states resulting from a pump-pulse, control-pulse sequence, using identical pulses as described in the text, with a time delay of 62.4 fs between pulses. Constructive interference increases the excited state occupancy to 4.3%.

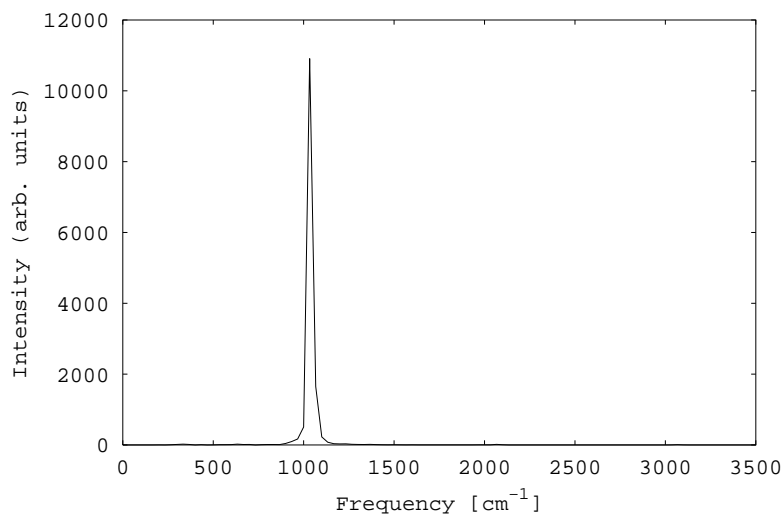


Figure 38: Fourier power spectrum for a one picosecond simulation following the control pulse. Notice the enormous enhancement of the breathing-mode vibration, by more than a factor of 20 when compared to Fig. 35.

inated by the breathing-mode vibration, which is typical of systems excited by ultrashort laser pulses with an intensity high enough to produce significant absorption.

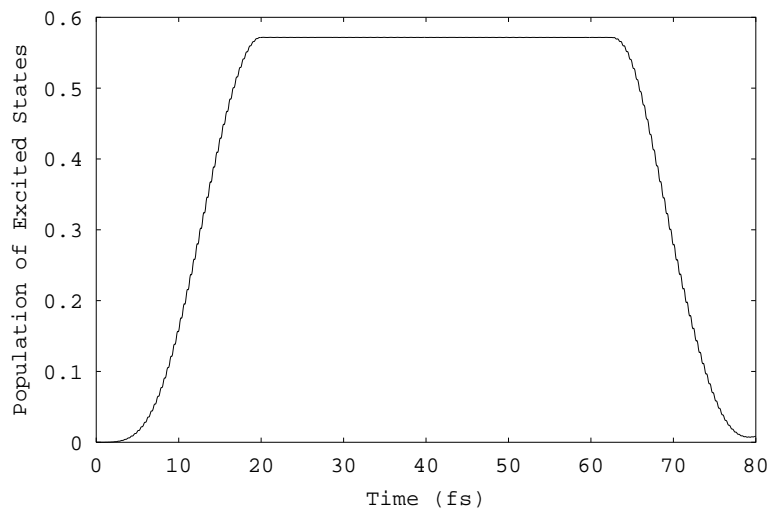


Figure 39: Population of the excited states resulting from a pump-pulse, control-pulse sequence, using identical pulses as described in the text, with a time delay of 62.8 fs between them. Destructive interference leads to a depopulation of the excited states, so that only $2 \times 10^{-2}\%$ of the electrons are left in these states.

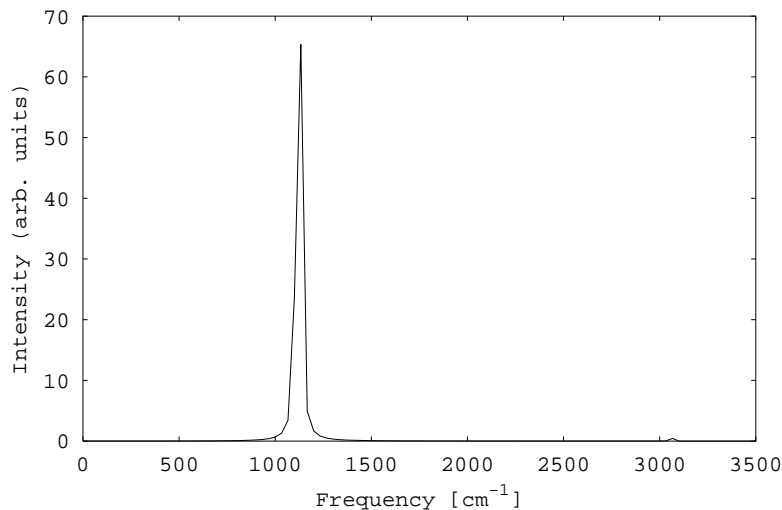


Figure 40: Fourier power spectrum for a one picosecond simulation following the control pulse, which was delayed by an interval chosen to depopulate the excited states but retain the breathing-mode vibration. The breathing-mode amplitude was decreased by a factor of 7 compared to Fig. 35, but is still appreciable.

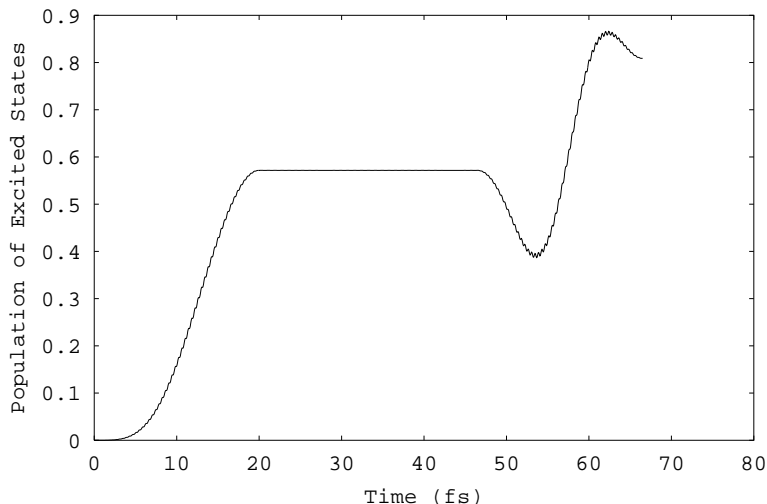


Figure 41: Population of the excited states resulting from a pump-pulse, control-pulse sequence using identical pulses, as described in the text, with a time delay of 46.8 fs between pulses. Destructive interference leading to a depopulation of the excited states might have been expected, but the actual result is a net increase of roughly 40% in the excited-state electron occupancy. As explained in the text, this is due to a very interesting subtlety involving a Jahn-Teller distortion and splitting of initially-degenerate and partially-occupied excited states.

The condition for constructive interference, viewed in the simplest way, is that the delay in time between the phase-locked pump pulse and control pulse should be an integer multiple of the characteristic period of vibration. Fig. 36 is a close-up view of Fig. 34 for 40 fs following the completion of the pump pulse. Notice the structure in the excited-state occupancy. A Fourier transform reveals that the motion is dominated by two characteristic periods. They are 0.8 fs, which is the period of vibration of the pump pulse, and 31.2 fs, which corresponds to the period of the breathing-mode vibration. Therefore, if we want the control pulse to constructively interfere with the electronic excitation as well as the breathing-mode vibration, the delay between the pulses should be an integer multiple of both of these periods. A delay of 62.4 fs satisfies this condition.

The result of a pump-pulse, control-pulse sequence using identical pulses as described above, with a time delay of 62.4 fs between the pulses, does indeed reveal constructive interference. This sequence leads to a greater population of the excited states, as can be seen in Fig. 37, with 4.3% of the electrons now occupying the excited states. Fig. 38 shows the Fourier power spectrum for a one picosecond simulation following the control pulse. Notice the enormous enhancement of the breathing-mode vibration, by more than a factor of 20 when compared to Fig. 35.

To examine the degree to which we can control the population of excited states, we changed the delay between the two pulses to 62.8 fs, an increase of only 0.4 fs. With this

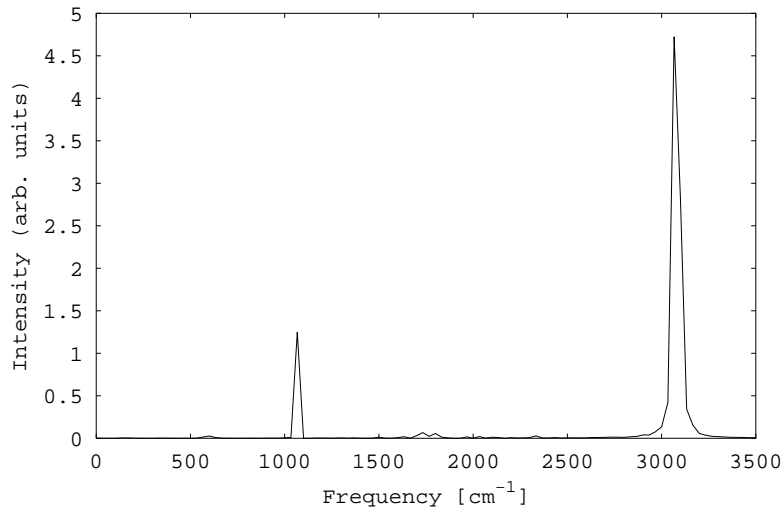


Figure 42: Fourier power spectrum for a one picosecond simulation, following a control pulse whose delay was chosen to both depopulate the excited states and suppress the breathing-mode. The breathing-mode amplitude is decreased by a factor of 400 when compared to Fig. 35, whereas the amplitude of the beating mode is relatively unaffected.

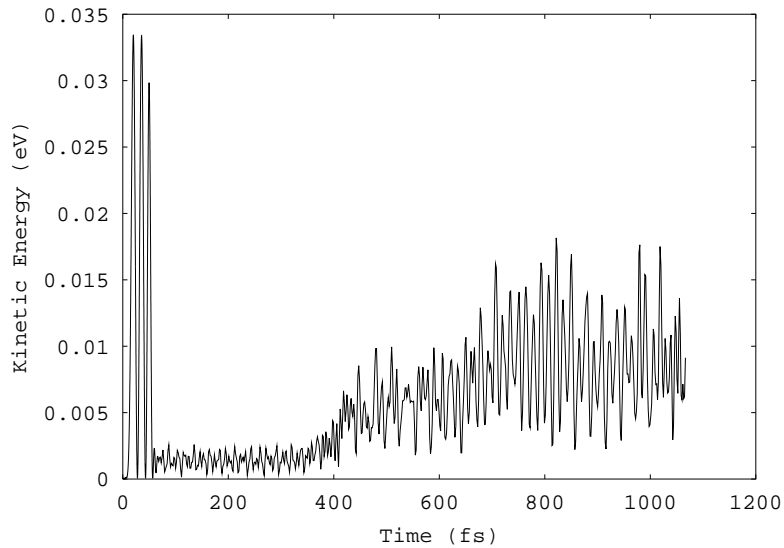


Figure 43: The kinetic energy as a function of time for a pump-pulse, control-pulse sequence with the control-pulse time-delayed by 46.8 fs. The kinetic energy is greatly diminished by the control pulse. However, some kinetic energy is regained after about 400 fs through a Jahn-Teller distortion of the occupied excited states.

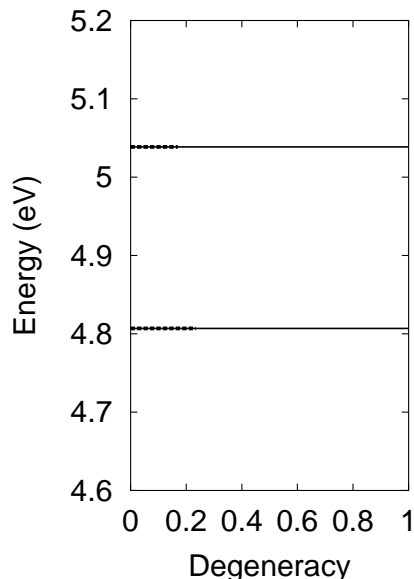


Figure 44: Energies of two originally degenerate excited states in a benzene molecule, following a pump-pulse, control-pulse sequence, with the control-pulse time-delayed by 46.8 fs. These states were degenerate at the completion of the control pulse, but a Jahn-Teller distortion then splits the levels by about 0.2 eV, with approximately 33% greater occupancy for the lower level.

delay we would expect to get destructive interference, resulting in a decrease in the excited-state occupancy. However, this time delay should still give constructive interference for the breathing mode, since the ratio of the delay to the breathing-mode period is $62.8/31.2 = 2.013$. The results for the excited-state electron occupancy are shown in Fig. 39, which clearly reveals that the result of the control pulse was to depopulate the excited states, leaving only about $2 \times 10^{-2}\%$ of these states occupied. The effect on the vibrations is shown in Fig. 40, which shows that this vibration was decreased by a factor of 7 when compared to the simulation with no control pulse, even though one might have expected that this commensurate time delay would increase the breathing-mode amplitude. Nevertheless, this chosen pump-pulse, control-pulse sequence has left the system with virtually no occupation of the excited states, while having a far smaller effect on the coherent breathing mode.

We now consider the results of a pump-pulse, control-pulse simulation with a time delay of 46.8 fs, which, in the simple picture involving destructive interference, should depopulate the excited states as well as suppress the breathing-mode vibration. The results for the population of excited states are shown in Fig. 41. Although the population begins to decrease at the onset of the control pulse, it starts to rise approximately halfway through the pulse, and at the end there is a net increase in the excited-state population of roughly 40%. Detailed study reveals a subtlety behind this phenomenon, which demonstrates that the interplay of electron and ion dynamics can be surprisingly complex. If we look at

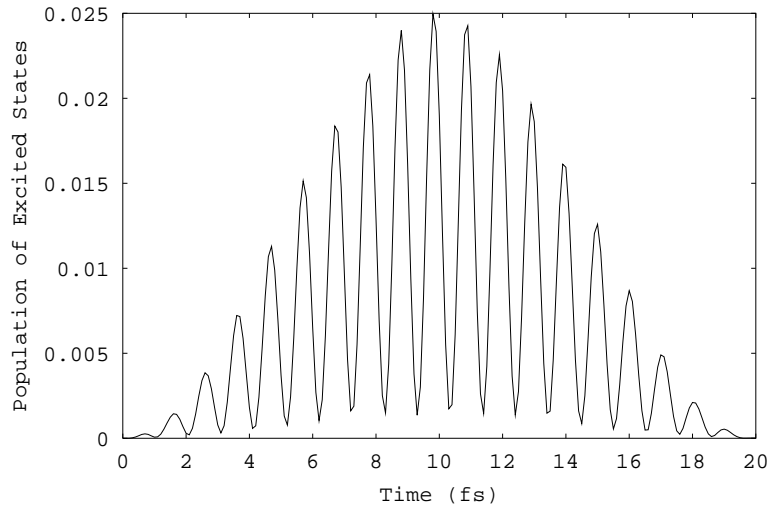


Figure 45: Electron population of the excited states resulting from a 10 fs FWHM laser pulse, centered at 2.0 eV and with a fluence of 1.1×10^{-2} KJ/m². Notice that there is no net occupancy of the excited states at the end of the pulse.

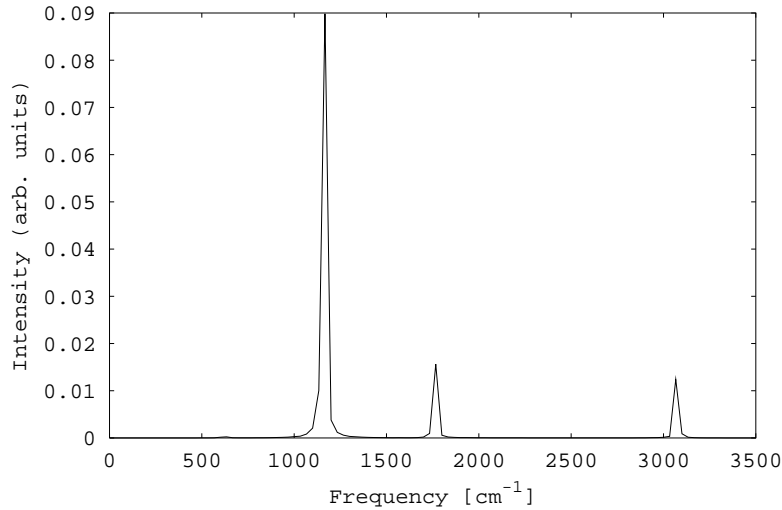


Figure 46: Fourier power spectrum of a one picosecond simulation following a 10 fs FWHM laser pulse, centered at 2.0 eV with a fluence of 1.1×10^{-2} KJ/m².

the Fourier power spectrum in Fig. 42, we see that the control was extremely effective in decreasing the intensity of the breathing-mode vibration, reducing it by a factor of nearly 400. Furthermore, if we look at the kinetic energy during this simulation, as shown in

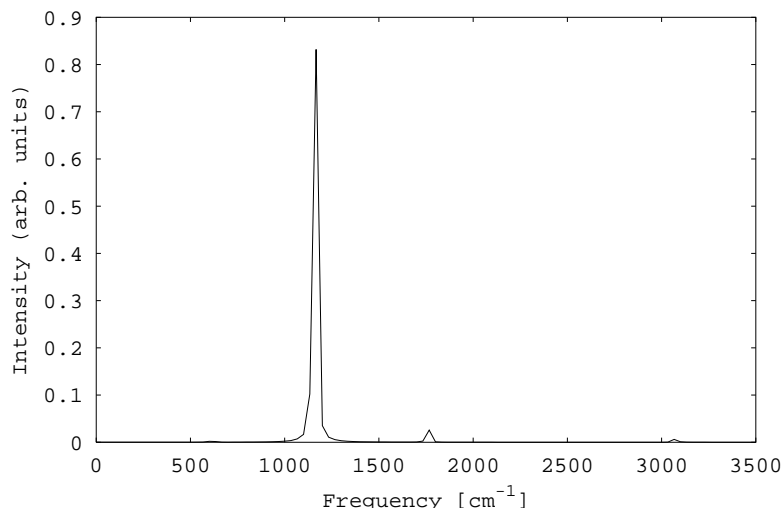


Figure 47: Fourier power spectrum for a one picosecond simulation following a pump-pulse, control-pulse sequence, using two identical laser pulses of 10 fs FWHM duration, centered at a photon energy of 2.0 eV, and with a fluence of 1.1×10^{-2} KJ/m². The control pulse was delayed by 63.14 fs in order to enhance the breathing mode. One can see that there is indeed an order-of-magnitude increase in the breathing mode amplitude as compared to Fig. 46.

Fig. 43, we see that initially this quantity was dramatically decreased, since most of it was associated with the breathing-mode vibration. However, following the control pulse there is a significant occupancy of the initially-degenerate excited states. The result is a Jahn-Teller distortion which splits these two levels by approximately 0.2 eV, with approximately 33% greater occupancy of the lower level, as shown in Fig. 44.

These coherent-control simulations for benzene have thus provided a clear demonstration of the complex interplay between electronic excitations and molecular vibrations.

Finally, we show how depopulation of excited states, after the laser pulse is complete, can lead to control of the vibrational motion for ultrashort nonresonant pulses. Fig. 45 is a plot of the electron population of the excited states following a 10 fs FWHM laser pulse, centered at a photon energy of 2.0 eV, with a fluence of 1.1×10^{-2} KJ/m². Notice that there is no net occupation of the excited states at the end of the pulse. The resulting Fourier power spectrum, for a simulation of one picosecond following the laser pulse, is shown in Fig. 46. If we now use two identical pulses in a pump-pulse, control-pulse sequence, time-delayed by 63.14 fs, we obtain constructive interference for the breathing-mode vibration. As can be seen in Fig. 47, there is an order-of-magnitude increase in the excitation of this mode. On the other hand, if we delay the control pulse by 77.63 fs, in order to achieve destructive interference for the breathing mode, we get the result shown in Fig. 48: a decrease in the breathing-mode amplitude by more than a factor of 10. Notice also that the control of the breathing mode, over a range of more than 2 orders of magnitude, has been attained with

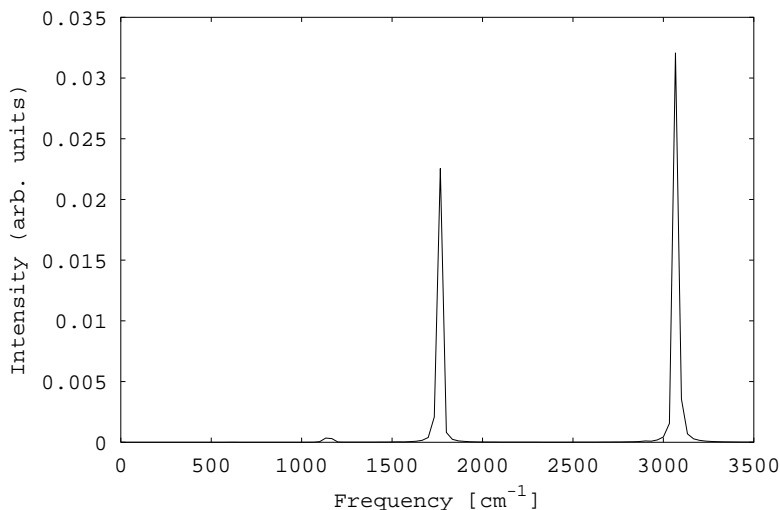


Figure 48: Fourier power spectrum for a one picosecond simulation following a pump-pulse, control-pulse sequence using two identical laser pulses of 10 fs FWHM duration, centered at 2.0 eV with a fluence of 1.1×10^{-2} KJ/m². The control pulse was delayed by 77.63 fs in order to diminish the breathing mode. One can see that there is more than an order of magnitude decrease in the breathing mode amplitude as compared to Fig. 46.

essentially no effect on the other vibrational modes.

8 Conclusion

In this paper we studied the following specific problems:

(1) Photoinduced cycloaddition of ethylene molecules. When two ethylene molecules approach each other in the ground state as in Figs. 5 and 6, they do not react even at high energy. After absorption of laser radiation, however, one molecule is in a more reactive excited state, and a strongly attractive bonding interaction is observed in our simulations. One can see in Fig. 10 that the molecules are in fact pulled together quickly by this interaction.

(2) Selective photodissociation of cyclobutane. In Fig. 14, the cyclobutane molecule cleanly separates into two ethylene molecules. Moreover, with the present approach one can monitor the detailed behavior on a femtosecond time scale. We found that the reaction proceeds through a tetramethylene reaction intermediate, as portrayed in Fig. 12 and actually observed in Fig. 14.

(3) Photoisomerization of butadiene. Both the trans-to-cis and cis-to-trans isomerizations were observed in our simulations. All the features of the molecular motion during the transition can be studied in detail – for example, a rotation about the carbon-carbon bond in Fig. 24.

(4) Two-pulse coherent control of benzene. One can enhance the population of excited electrons, as in Fig. 37, or drive them back to the ground state, as in Fig. 39. One can also

greatly enhance specific vibrational modes, as in Fig. 38, or greatly suppress them, as in Fig. 42.

These results demonstrate that it is possible to perform realistic simulations of molecules responding to laser pulses, and that such simulations can provide genuine guidance toward achieving the goal of laser control of chemical reactions.

Acknowledgement

This work was supported by the Robert A. Welch Foundation.

References

- [1] W. S. Warren, H. Rabitz, and M. Dahleh, *Science* **259**, 1581 (1993).
- [2] J. S. Graves and R. E. Allen, *Phys. Rev. B* **58**, 13 627 (1998).
- [3] T. Dumitrică and R. E. Allen, *Solid State Commun.* **113**, 653 (2000).
- [4] T. Dumitrica, B. Torralva, and R. E. Allen, in *The Optical Properties of Materials*, edited by J. Chelikowsky, S. Louie, G. Martinez, and E. Shirley (Materials Research Society, Warrendale, Pennsylvania, 2000).
- [5] R. E. Allen, T. Dumitrica, and B. Torralva, Chapter 7 of *Ultrafast Physical Processes in Semiconductors*, edited by K. T. Tsen (Academic, New York, 2001).
- [6] B. R. Torralva, Ph. D. dissertation, Texas A&M University (May, 2001).
- [7] B. Torralva, T. Niehaus, M. Elstner, Th. Frauenheim, S. Suhai, and R. E. Allen, to be published.
- [8] B. Torralva and R. E. Allen, to be published.
- [9] D. Porezag, Th. Frauenheim, Th. Köhler, G. Seifert, and R. Kaschner, *Phys. Rev. B.* **51**, 12947 (1994).
- [10] Th. Frauenheim, F. Weich, Th. Köhler, S. Uhlmann, D. Porezag, and G. Seifert, *Phys. Rev. B* **52**, 11492 (1995).
- [11] A. Sieck, D. Porezag, Th. Frauenheim, M. R. Pederson, and K. Jackson, *Phys. Rev. A* **56**, 4890 (1997).
- [12] M. Elstner, D. Porezag, G. Jungnickel, J. Elsner, M. Haugk, Th. Frauenheim, S. Suhai, and G. Seifert, *Phys. Rev. B* **58**, 7260 (1998).
- [13] R. B. Woodward and R. Hoffmann, *The Conservation of Orbital Symmetry* (Academic press, 1970).
- [14] R. Hoffmann, S. Swaminathan, B. G. Odell, and R. Gleiter, *J. Am. Chem. Soc.* **92**, 7091 (1970).
- [15] S. Pedersen, J. L. Herek, and A. H. Zewail, *Science* **266**, 1359 (1994).
- [16] R. A. Mathies, *Novartis Foundation Symposium 226: Rhodopsin & Phototransduction* (John Wiley & Sons, 1999).
- [17] S. W. Lin, M. Groesbeek, I. van der Hoef, P. Verdegem, J. Lugtenburg, and R. A. Mathies, *J. Phys. Chem. B* **102**, 2787 (1998).
- [18] G. Müller, K. K. Gneuss, H.-P. Kriemler, A. I. Scott, and A. J. Irwin, *J. Am. Chem. Soc.* **101**, 3658 (1979).

- [19] M. Hase, K. Mizoguchi, H. Harima, S. Nakashima, M. Tani, K. Sakai, and M. Hangyo, *Appl. Phys. Lett.* **69**, 2474 (1996).
- [20] A. P. Heberle, J. J. Baumberg, and K. Köhler, *Phys. Rev. Lett.* **75**, 2598 (1995).
- [21] E. H. Hertz, O. Faucher, B. Lavorel, F. DallaVia, and R. Chaux, *Phys. Rev. A* **61**, 33816 (2000).
- [22] E. D. Potter, J. L. Herek, S. Pedersen, Q. Liu, and A. H. Zewail, *Nature* **355**, 66 (1992).
- [23] A. P. Peirce, M. A. Dahleh, and H. Rabitz, *Phys. Rev. A* **37**, 4950 (1988).
- [24] J. L. Krause, R. M. Whitnel, K. R. Willson, Y. Yan, and S. Mukamel, *J. Chem. Phys.* **99**, 6563 (1993).
- [25] M. Shapiro, *J. Phys. Chem.*, **97**, 7396 (1993).
- [26] V. Blanchet, M. A. Bouchene, and G. Girard, *J. Chem. Phys.* **108**, 4862 (1998).
- [27] S. M. Park, S. P. Lu, and R. J. Gordon, *J. Chem. Phys.* **94**, 8622 (1991).
- [28] V. D. Kleiman, L. Zhu, H. Alen, and R. J. Gordon, *J. Chem. Phys.* **103**, 10800 (1995).